Chapter 2
Black Hole Masses and the M-sigma Relation

https://doi.org/10.1017/S1743921323002478 Published online by Cambridge University Press

Cosmic Masers: Proper Motion toward the Next-Generation Large Projects
Proceedings IAU Symposium No. 380, 2024
T. Hirota, H. Imai, K. Menten, & Y. Pihlström, eds.
doi:10.1017/S1743921323002478

Supermassive black hole mass growth in infrared-luminous gas-rich galaxy mergers and potential power of (sub)millimeter H_2O megamaser observations

Masatoshi Imanishi

National Astronomical Observatory of Japan, 2-21-1 Osawa Mitaka, Tokyo 181-8588, Japan.
email: masa.imanishi@nao.ac.jp

Abstract. We present our systematic infrared and (sub)millimeter spectroscopic observations of gas/dust-rich merging ultraluminous infrared galaxies (ULIRGs) to scrutinize deeply buried AGNs (mass-accreting supermassive black holes [SMBHs]). We have found signatures of optically elusive, but intrinsically luminous buried AGNs in a large fraction of nearby ($z < 0.3$) ULIRGs, suggesting that SMBH mass growth is ongoing in the ULIRG population. Using ALMA, we have detected compact (<100 pc), very luminous ($>10^4 L_\odot$), AGN-origin, 183 GHz (1.6 mm) H_2O megamaser emission in one merging ULIRG, demonstrating that the megamaser emission can be a very powerful tool to dynamically estimate SMBH masses, with the smallest modeling uncertainty of kpc-wide stellar and gas mass distribution, at dusty ULIRGs' nuclei, because of minimum extinction effects at millimeter. We present our current results and future prospect for the study of the SMBH mass growth in gas/dust-rich galaxy mergers, using (sub)millimeter AGN-origin H_2O megamaser emission lines.

Keywords. Supermassive black hole, Water megamaser, Ultraluminous infrared galaxies, Active galactic nuclei, Millimeter megamaser, Gas-rich galaxy mergers

1. Introduction: Co-evolution of stars and supermassive black holes in the universe

The apparent ubiquity of supermassive black holes (SMBHs) at the centers of present-day galaxies, and the correlation between the masses of SMBHs and spheroidal stars (e.g., Magorrian *et al.* 1998; Ferrarese & Merritt 2000; McConnell & Ma 2013) indicate that an active galactic nucleus (AGN; SMBH-driven activity) and a starburst (active star-formation; plausibly the progenitors of spheroids) are physically connected and have *co-evolved*. The widely accepted cold dark matter-based galaxy formation scenarios (e.g., White & Rees 1978) postulate that mergers of gas-rich galaxies with SMBHs at their centers are common throughout the history of the universe (Hopkins *et al.* 2008). Numerical simulations of such galaxy mergers predict that not only *many stars are formed* rapidly, but also *SMBHs grow in mass* through high mass accretion rates, at deeply embedded nuclear regions by gas and dust (Hopkins *et al.* 2006). Such gas/dust-rich galaxy mergers become infrared luminous and are usually observed as ultraluminous infrared galaxies (ULIRGs; infrared luminosity $L_{IR} > 10^{12} L_\odot$ †; Sanders & Mirabel (1996)). Thus, ULIRGs are believed to be an important phase for the growth of SMBH mass and the *co-evolution* of SMBHs and stars in the universe.

† Throughout this manuscript, we adopt the cosmological parameters $H_0 = 71$ km s^{-1} Mpc^{-1}, $\Omega_M = 0.27$, and $\Omega_\Lambda = 0.73$.

To discuss the SMBH mass growth in ULIRGs, it is crucial to estimate the energetic contributions from AGN activity (energetically dominated by a mass-accreting SMBH), by distinguishing from starburst activity which is powered by nuclear fusion inside stars. Unlike optically (0.3–1 μm) identifiable AGNs which are surrounded by toroidally distributed (torus-shaped) dusty medium (i.e., certain opening angle where ionizing UV photons can escape) (Baldwin *et al.* 1981; Veilleux & Osterbrock 1987; Kewley *et al.* 2001; Kauffmann *et al.* 2003), ULIRGs are major mergers of gas-rich galaxies and have large amounts of concentrated molecular gas and dust in nuclear regions (Sanders & Mirabel 1996). Putative compact AGNs at ULIRGs' nuclei can easily be obscured by gas and dust *in virtually all lines of sight* (i.e., almost no opening angle), and so optical detection of AGN signatures becomes extremely difficult. However, understanding the energetic importance of such optically elusive, but intrinsically luminous *buried* AGNs is vital to clarify the true nature of the ULIRG population (Hopkins *et al.* 2005) as well as the SMBH mass growth process during gas-rich galaxy mergers (Hopkins *et al.* 2008; DeBuhr *et al.* 2011), which must have happened very frequently in the early universe, if we are based on the widely accepted cold dark matter-based galaxy formation scenario (e.g., White & Rees 1978).

2. Observations at wavelengths of low extinction

It is well known from observations that nearby ($z < 0.3$) ULIRGs are energetically dominated by compact (<kpc) nuclear regions, rather than spatially extended (>a few kpc) star-formation in the host galaxies (e.g., Soifer *et al.* 2000; Diaz-Santos *et al.* 2010; Imanishi *et al.* 2011; Pereira-Santaella *et al.* 2021). It is of particular importance to distinguish between AGNs and compact nuclear starbursts, and estimate how they contribute energetically in nearby ULIRGs. Because AGNs (=mass-accreting SMBHs) are spatially more centrally concentrated than, and are surrounded by, compact nuclear starbursts in ULIRGs' nuclei, AGNs are generally more difficult to detect observationally. It is indispensable to observe at wavelengths of low dust extinction if we are to detect putative AGNs and properly estimate their energetic importance in dusty ULIRGs' nuclei. A buried AGN (mass-accreting SMBH) has two distinguished properties, when compared to a starburst (nuclear fusion inside stars). First, because the radiative energy generation efficiency of a mass-accreting SMBH (6–42% of $\dot{M}c^2$; Bardeen (1970); Thorne (1974)) is much higher than that of nuclear fusion inside stars ($\sim$0.7% of $\dot{M}c^2$), an AGN can produce very large luminosity from a compact region (i.e., high emission surface brightness) (Soifer *et al.* 2000; Thompson *et al.* 2005; Pereira-Santaella *et al.* 2021) and create a larger amount of hot (>100K) dust than a starburst can. Thus, an AGN can become luminous in the near- to mid-infrared (1–30 μm) because of this hot dust thermal radiation. Second, X-ray to UV luminosity ratio is substantially higher in an AGN than a starburst, because of strong X-ray emission in the vicinity of a mass-accreting SMBH through the inverse Compton upscattering of UV photons to X-rays (Ranalli *et al.* 2003; Shang *et al.* 2011). If we can detect at least one of these features characteristic to an AGN, then we can separate AGN and starburst activity, and estimate how an AGN energetically contributes to the bolometric luminosity of a ULIRG. From this information, we can convert to mass accretion rate onto a SMBH.

2.1. *X-rays*

Because an AGN is a much more luminous X-ray emitting source than a starburst, detection of intrinsically luminous X-ray emission can be the most straightforward way to argue for the presence of a luminous AGN. In particular, extinction effects become smaller at hard X-rays at >10 keV (e.g., Ryter 1996; Wilms *et al.* 2000). Thus, >10

https://doi.org/10.1017/S1743921323002478 Published online by Cambridge University Press

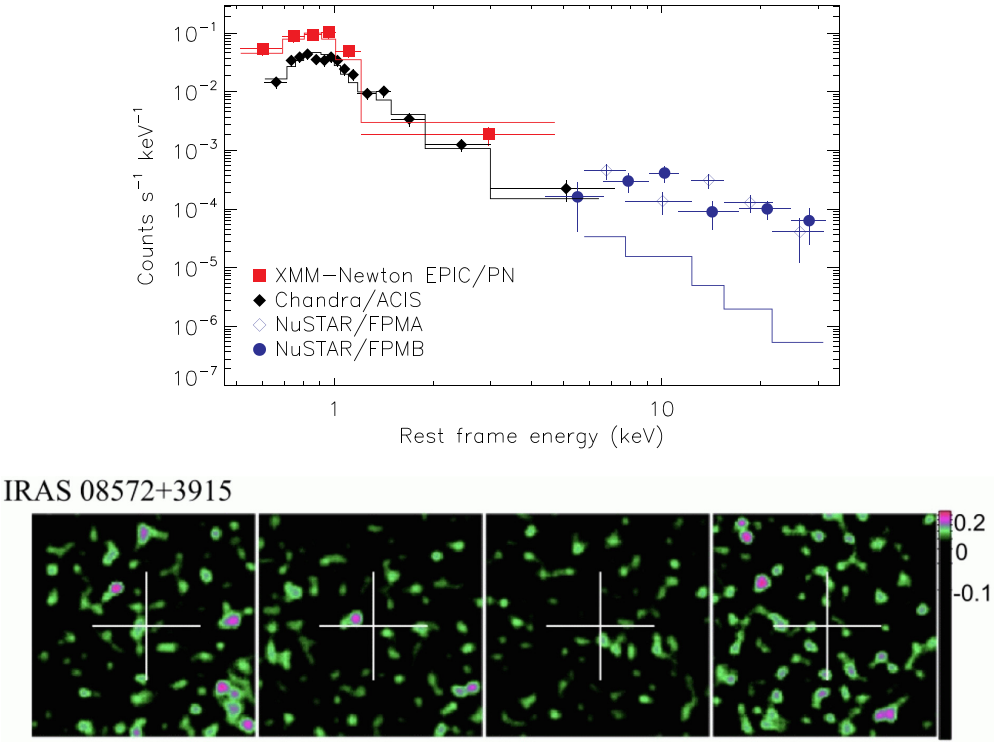

Figure 1. *(Top)*: X-ray spectrum of the LIRG NGC 6286 ($L = 10^{11.4} L_\odot$; $z = 0.018$). Compared to the extrapolation from 1–5 keV X-ray emission which is dominated by starburst activity, there is an excess component at >5 keV. This excess emission is interpreted as originating from highly absorbed, but intrinsically luminous AGN activity (Ricci *et al.* 2016). *(Bottom)*: X-ray image of the ULIRG IRAS 08572+3915 ($L = 10^{12.1} L_\odot$; $z = 0.058$) at *(Left)* 3–10 keV, *(Second left)* 10–20 keV, *(Second right)* 20–30 keV, and *(Right)* 30–79 keV (Teng *et al.* 2015). This ULIRG has no optical AGN signature, but is classified as buried AGN dominated in infrared spectroscopy (as we will explain later; see Figure 2 bottom middle). However, no significant X-ray emission is detected at >10 keV at the position of this ULIRG shown as the cross mark.

keV hard X-ray observations can be an effective tool to detect deeply buried AGNs by penetrating through a large column density of obscuring material at ULIRGs' nuclei. In fact, these hard X-ray observations have been successful to detect highly absorbed, but intrinsically luminous, X-ray emitting AGNs in a few luminous infrared galaxies (LIRGs; $L_{IR} = 10^{11-12} L_\odot$) and ULIRGs (e.g., Ricci *et al.* 2016, 2017; Oda *et al.* 2017; Yamada *et al.* 2021). An example is shown in Figure 1 (top). However, detection of >10 keV hard X-ray emission from ULIRGs has been unsuccessful in many cases, even for very nearby sources at $z < 0.1$ (e.g., Teng *et al.* 2015) (Figure 1 bottom). It is possible that these hard X-ray non-detected ULIRGs do not contain luminous AGNs and are starburst dominated. However, it is also possible that the putative buried AGNs in these ULIRGs suffer from heavily Compton thick X-ray absorption with hydrogen column density $N_H > 5 \times 10^{25}$ cm^{-2}, in which case detection of X-ray emission is extremely difficult even at >10 keV.

2.2. *Infrared*

Infrared 2.5–35 μm low-resolution spectroscopy is another powerful tool to detect deeply buried, but intrinsically luminous AGNs in nearby ($z < 0.3$) ULIRGs, because of

https://doi.org/10.1017/S1743921323002478 Published online by Cambridge University Press

much reduced dust extinction effects compared to the optical (0.3–1 μm). Furthermore, spectroscopy at this infrared wavelength range can distinguish between AGNs and starbursts, based on polycyclic aromatic hydrocarbon (PAH) emission and broad dust absorption features, as long as buried AGNs contribute significantly to observed infrared fluxes (Figure 2). This infrared spectroscopic energy diagnostic method has been applied to >100 nearby ULIRGs at $z < 0.3$ and been successful to detect luminous buried AGNs in roughly half of the observed nearby ULIRGs (e.g., Genzel *et al.* 1998; Imanishi *et al.* 2006a; Armus *et al.* 2007; Imanishi *et al.* 2007a, 2008; Nardini *et al.* 2008; Imanishi 2009; Veilleux *et al.* 2009; Nardini *et al.* 2009, 2010; Imanishi *et al.* 2010a,b). Most importantly, in this infrared spectroscopy, luminous buried AGN signatures have been found in many nearby ULIRGs with no AGN signatures in hard X-rays at 10–80 keV (Figure 1 bottom), due to heavily Compton thick X-ray absorption ($N_H > 5 \times 10^{25}$ cm^{-2}). This is because the ratios of X-ray absorption (N_H by gas and dust) to infrared dust extinction (A_V) toward obscured AGNs are known to be much higher than the Galactic value of $N_H/A_V \sim 2 \times 10^{21}$ cm^{-2} mag^{-1} (Predehl & Schmitt 1995), most likely because of the presence of large amount of dust-free X-ray absorbing gas inside the dust sublimation radius around AGNs (e.g., Alonso-Herrero *et al.* 1997; Burtscher *et al.* 2015; Ichikawa *et al.* 2019). Thus, infrared spectroscopy has turned out to be more effective than hard X-ray observations to detect deeply buried AGNs in nearby ULIRGs.

However, there remain many nearby ULIRGs which do not display buried AGN signatures in the infrared. It may be possible that these ULIRGs do not contain luminous AGNs. However, another scenario is that the putative buried AGNs can be even infrared elusive because of extremely high obscuration. In fact, there are arguments that a certain fraction of nearby ULIRGs' nuclei are so dusty that opacity toward the putative buried AGNs can become very large (optical depth $\tau > 1$) at infrared 2.5–35 μm (e.g., Downes & Eckart 2007; Sakamoto *et al.* 2008; Matsushita *et al.* 2009; Gonzalez-Alfonso *et al.* 2015; Scoville *et al.* 2017; Sakamoto *et al.* 2021; Pereira-Santaella *et al.* 2021). It is indispensable to observe at wavelengths of even lower extinction effects than 2.5–35 μm, if we are to distinguish between these two scenarios.

2.3. *(Sub)millimeter*

Extinction effects at (sub)millimeter 0.8–3.5 mm are a factor of >20 smaller than those at infrared 2.5–35 μm (Hildebrand 1983). Thus, (sub)millimeter observations can have a potential to detect infrared-elusive, extremely deeply buried AGNs in nearby ULIRGs. Then, how can we distinguish between an AGN and a starburst at (sub)millimeter? Because a luminous AGN can show much stronger X-ray and near- to mid-infrared (1–30 μm) hot (>100 K) dust emission than a starburst can, physical and chemical effects to surrounding molecular gas can be different depending on energy sources (e.g., Meijerink *et al.* 2007; Harada *et al.* 2010). Thus, molecular rotational J-transition emission line flux ratios can be different between an AGN and a starburst. If we find AGN-sensitive bright molecular J-transition lines in the (sub)millimeter wavelength range, we have a tool to detect infrared-elusive extremely deeply buried luminous AGNs in gas/dust-rich merging ULIRGs, by distinguishing from starbursts. Because ULIRG's nuclear regions are usually dominated by high density molecular gas, caused by merger-induced gas compression (Gao & Solomon 2004), molecules with large dipole moments, such as HCN, HCO^+, HNC ($\mu \gtrsim 3$ debye; C means ^{12}C throughout this manuscript), are better suited than widely used bright low-J ($J \lesssim 3$) lines of CO ($\mu = 0.1$ debye), to properly probe the physical and chemical properties of ULIRG's nuclear dense molecular gas. Pre-ALMA millimeter observations found a clear trend that optically identified luminous AGNs display higher HCN-to-HCO^+ flux ratios than starburst-dominated galaxies, at J=1–0 (rotational transition) at ∼3.5 mm (e.g., Kohno 2005; Krips *et al.* 2008). Enhanced HCN

https://doi.org/10.1017/S1743921323002478 Published online by Cambridge University Press

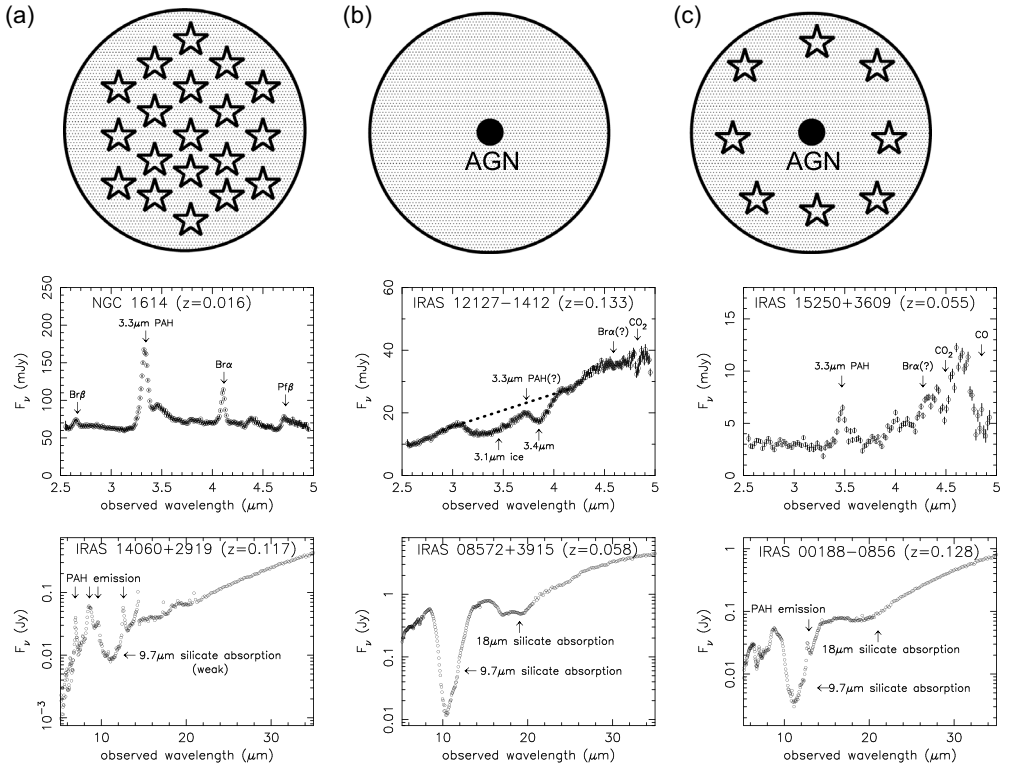

Figure 2. Infrared 2.5–35 μm low-resolution (R = 50–100) spectroscopic energy diagnostic method of galaxies, using polycyclic aromatic hydrocarbon (PAH) emission and dust absorption features (Imanishi *et al.* 2007a, 2008, 2010a). *(Top)*: Primary energy source and its geometry. *(Left)*: A pure starburst galaxy. Stellar energy sources and dust/gas are spatially well mixed. Prominent, large equivalent width, PAH emission features, excited by stellar far-UV photons in photo-dissociation regions, are found in infrared 2.5–35 μm spectra. The optical depths of dust absorption features are modest in this mixed dust/source geometry, because the observed flux largely comes from foreground, weakly obscured emission at a near side (which shows only weak dust absorption features), with small contributions from highly obscured emission at a far side (which can display deep dust absorption features). *(Middle)*: A pure buried AGN. The energy source (a mass-accreting SMBH) is more centrally concentrated than the surrounding dust. No PAH emission feature is seen, because PAH molecules are destroyed by strong AGN's X-ray radiation, in regions where PAH-exciting AGN's far-UV photons are available. PAH-free continuum emission from larger-sized hot (>100 K) dust heated by an AGN is dominant. The optical depths of dust absorption features can be very large in this centrally concentrated energy source geometry, because the so-called foreground screen dust model is applicable. *(Right)*: A buried AGN and starburst composite galaxy. PAH emission from starburst regions is seen, but its equivalent width is lower than a pure starburst-dominated galaxy, because of the dilution by AGN-originating PAH-free continuum emission. *(Second row)*: Infrared 2.5–5 μm spectra taken with the AKARI infrared satellite (Imanishi *et al.* 2008, 2010a). The 3.3 μm PAH emission feature is prominent in a starburst *(Left)*, but is weak in buried AGNs *(Middle and Right)*. The 3.1 μm and 3.4 μm absorption features come from ice-covered dust and bare carbonaceous dust, respectively. The red, steeply rising continuum flux with increasing wavelength, caused by hot dust thermal emission, also suggests the presence of a luminous buried AGN *(Middle and Right)*. Hydrogen recombination lines (Brα at 4.05 μm, Brβ at 2.63 μm, and Pfβ at 4.65 μm) can be strongly emitted in HII-regions in a starburst *(Left)*. Absorption features by CO_2 (at 4.26 μm) and/or CO (at 4.67 μm) are also seen for ULIRGs containing deeply buried AGNs *(Middle and Right)*. *(Bottom)*: Infrared 5–35 μm spectra taken with the Spitzer infrared satellite (Imanishi *et al.* 2007a). PAH emission features at 6.2 μm, 7.7 μm, 8.6 μm, and 11.3 μm, are prominent in a starburst *(Left)*, but are weak in buried AGNs *(Middle and Right)*. The 9.7 μm and 18 μm silicate dust absorption features can be strong in buried AGNs *(Middle and Right)*, but are weak in a starburst *(Left)*. All (L)LIRGs plotted in this figure do not display obvious AGN signatures in optical spectra (optically classified as HII-regions or LINERs).

https://doi.org/10.1017/S1743921323002478 Published online by Cambridge University Press

abundance caused by AGN radiation and/or mechanical effects is regarded to be responsible for the elevated HCN emission in luminous AGNs (e.g., Kohno 2005; Izumi *et al.* 2013; Krips *et al.* 2008; Aladro *et al.* 2015; Saito *et al.* 2018; Nakajima *et al.* 2018; Takano *et al.* 2019; Kameno *et al.* 2020; Imanishi *et al.* 2020; Butterworth *et al.* 2022; Imanishi *et al.* 2023). This HCN-to-HCO^+ flux ratio method was applied to nearby ULIRGs, and it was demonstrated that ULIRGs with infrared-classified luminous buried AGNs tend to display higher HCN-to-HCO^+ flux ratios than known starburst-dominated galaxies at J=1–0 (e.g., Imanishi *et al.* 2006b, 2007b, 2009; Privon *et al.* 2015), at J=2–1 (e.g., Imanishi *et al.* 2022), at J=3–2 (e.g., Imanishi *et al.* 2016b, 2019) (Figure 3 bottom left), and at J=4–3 (e.g., Izumi *et al.* 2016; Imanishi *et al.* 2018) (Figure 3 top). In Figure 3 (bottom right), we plot the observed HCN-to-HCO^+ flux ratios at J=3–2 in the ordinate, as a function of infrared-estimated AGN's bolometric contributions (Nardini *et al.* 2010) in the abscissa. Not only infrared-identified luminous buried AGNs, but also infrared-classified starbursts, without luminous buried AGN signatures in the infrared, display high HCN-to-HCO^+ flux ratios with larger than unity, as expected for AGN-important galaxies. If the high HCN-to-HCO^+ flux ratios are a reliable AGN indicator, then this result may suggest that (i) almost all nearby ULIRGs contain luminous AGNs (i.e., mass-accreting SMBHs), and (ii) SMBH-mass growth is ubiquitous in the nearby ULIRG population. In this case, our next desire is to estimate SMBH mass and directly witness the SMBH mass growth in nearby gas/dust-rich merging ULIRGs.

3. H_2O megamaser emission and direct SMBH mass measurements in gas/dust-rich infrared luminous galaxy mergers

3.1. *Need for SMBH measurements at extinction free wavelengths*

It is *inferred* from host galaxies' stellar properties that SMBH masses in nearby ULIRGs can be as high as $M_{SMBH} = 10^{7-8} M_\odot$ (e.g., Genzel *et al.* 2001; Dasyra *et al.* 2006). It is crucial to verify this more directly. Investigating the dynamics of gas and/or stars at galaxy nuclear regions that are largely affected by the gravity of a SMBH, is one of the most direct and reliable methods to estimate the central SMBH mass (e.g., Miyoshi *et al.* 1995). Many dynamical studies of gas and/or stars at the nuclei of *less obscured galaxies* have been conducted to estimate the central SMBH masses, mostly in the optical (0.3–1 μm) and near-infrared (1–2.5 μm) wavelength ranges (e.g., Kormendy & Ho 2013). However, these conventional optical and near-infrared methods are not applicable to ULIRGs' nuclei, because of very large dust extinction. It is urgently needed to establish a solid method to probe the dynamics of material around mass-accreting SMBHs at dusty ULIRGs' nuclei, at almost-dust-extinction-free wavelengths.

As described before, dust extinction effects in the (sub)millimeter wavelength (0.8–3.5 mm) are much smaller than the optical and near-infrared, and even smaller than other widely explored wavelengths of small dust extinction, ∼10 keV hard X-rays and infrared ∼20 μm, by a factor of >20 (Hildebrand 1983). Furthermore, possible free-free absorption effects by ionized gas ($\propto \lambda^{2.1}$), which are sometimes significant in the centimeter wavelength (1–22 cm) at ULIRGs' nuclei (e.g., Leroy *et al.* 2011; Murphy *et al.* 2013), are usually negligible at (sub)millimeter. (Sub)millimeter observations of molecular rotational transition lines can thus potentially be the most powerful means to investigate the dynamics of gas around mass-accreting SMBHs at ULIRGs' nuclei, by penetrating through a large column density of gas and dust.

3.2. *H_2O megamaser emission*

H_2O has more complex rotational energy levels than simple molecules (e.g., CO, HCN, HNC) and it was theoretically predicted that population inversion can occur for a

https://doi.org/10.1017/S1743921323002478 Published online by Cambridge University Press

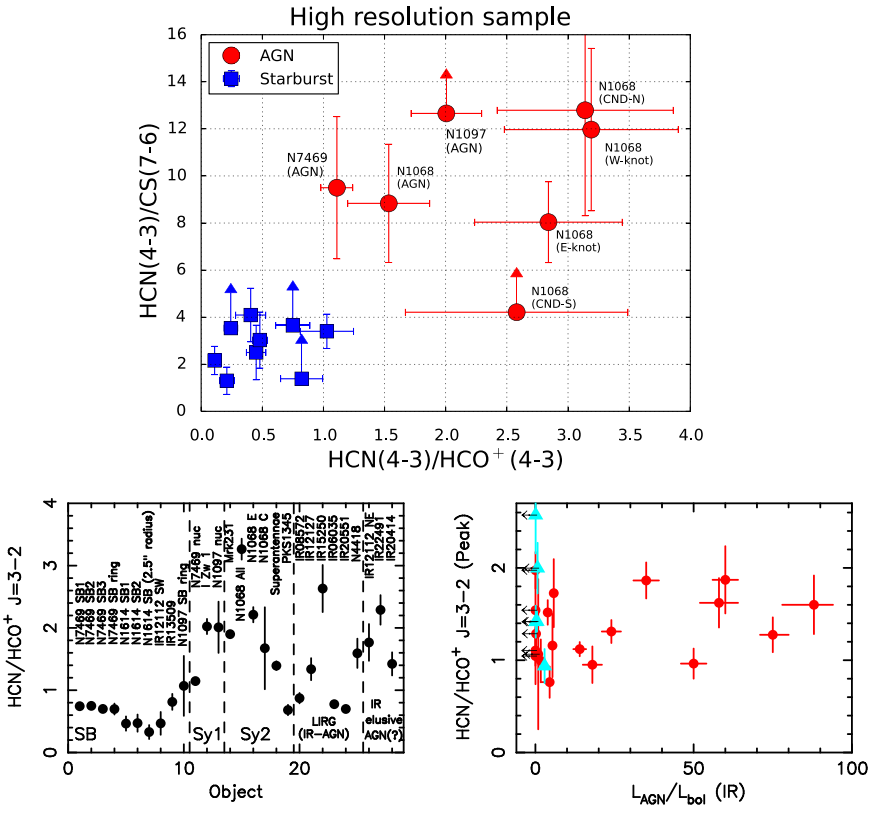

Figure 3. *(Top)*: Observed HCN-to-HCO^+ flux ratio at J=4–3 (abscissa) and HCN J=4–3 to CS J=7–6 flux ratio for galaxy nuclei observed with modestly high angular resolution (Izumi *et al.* 2016). AGN-important galaxies (red filled circles) tend to show higher HCN-to-HCO^+ flux ratios at J=4–3 than starburst-dominated galaxies (blue filled squares) in the abscissa. *(Bottom left)*: Observed HCN-to-HCO^+ flux ratios at J=3–2 (Imanishi *et al.* 2016b). "SB", "Sy1", "Sy2", "LIRG (IR-AGN)", and "IR elusive AGN(?)" mean starburst-dominated regions, optically identified Seyfert 1 type unobscured AGNs, optically identified Seyfert 2 type obscured AGNs, luminous infrared galaxies with optically elusive, but infrared-detected, buried AGN signatures, and candidates of infrared-elusive, but (sub)millimeter-detected, extremely deeply buried AGNs, respectively. Sources with AGN signatures tend to show elevated HCN-to-HCO^+ flux ratios, compared to starbursts. Some AGN-classified sources display non-high HCN-to-HCO^+ flux ratios, which can be explained by higher HCN flux attenuation by larger line opacity (not dust extinction), caused by enhanced HCN abundance in AGNs (Imanishi *et al.* 2016a,b). Optically thin ^{13}C isotopologue $H^{13}CN$-to-$H^{13}CO^+$ flux ratios are needed to remove the ambiguity coming from the possibly larger line opacity for HCN ($H^{12}CN$) than for HCO^+ ($H^{12}CO^+$). *(Bottom right)*: Comparison of infrared spectroscopically estimated AGN bolometric contribution (in %) by Nardini *et al.* (2010) (abscissa) and observed HCN-to-HCO^+ J=3–2 flux ratio at the nuclear continuum peak position within observed beam size (ordinate) in nearby ULIRGs (Imanishi *et al.* 2019). ULIRGs observed with small (0.1″–0.2″) beam sizes are plotted as red circles. Those observed with large (0.5″–0.9″) beam sizes are plotted as light blue triangles.

number of H_2O rotational transitions (e.g., 22 GHz $6_{1,6}$–$5_{2,3}$, 183 GHz $3_{1,3}$–$2_{2,0}$, and 321 GHz $10_{2,9}$–$9_{3,6}$ lines) through collisional excitation and/or infrared radiative pumping in AGN-illuminated warm and dense molecular gas (e.g., Neufeld *et al.* 1991; Yates *et al.* 1997; Maloney *et al.* 2002; Gonzalez-Alfonso *et al.* 2010; Gray *et al.* 2016). This population inversion can amplify background radiation and these *H_2O emission lines can be extremely bright* and high surface brightness *through maser phenomena*. In fact, H_2O

https://doi.org/10.1017/S1743921323002478 Published online by Cambridge University Press

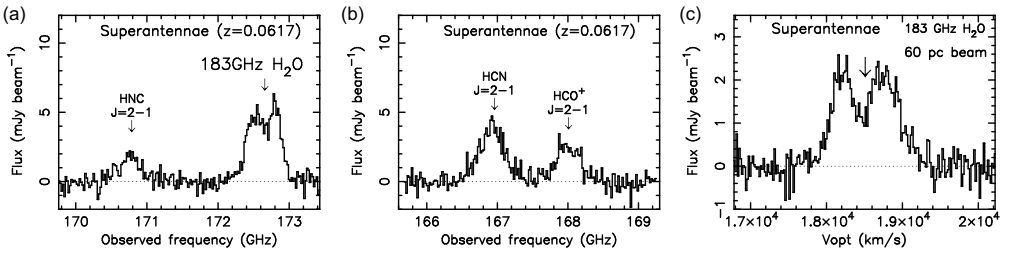

Figure 4. ALMA spectrum of the Superantennae for *(a)* HNC J=2–1 and 183 GHz H_2O lines and *(b)* HCN and HCO^+ J=2–1 lines, taken with ∼0.4″ (∼500 pc) beam (Imanishi *et al.* 2021). The abscissa is observed frequency (in GHz) and the ordinate is flux density (in mJy $beam^{-1}$). The *183 GHz H_2O emission line flux is even higher* than bright dense molecular gas tracers (HNC, HCN, and HCO^+ J=2–1 lines). *(c)*: Detailed velocity profile of the 183 GHz H_2O emission line in a newly taken ∼60 pc beam-sized spectrum (Imanishi *et al.* 2023b in preparation). The abscissa is optical LSR velocity (in km s^{-1}). The downward arrow indicates the systemic velocity (18510 km s^{-1}).

megamaser (>$10L_\odot$) emission was detected in many AGNs at 22 GHz (1.4 cm) through previously conducted centimeter observations (e.g., Braatz *et al.* 1997; Hagiwara *et al.* 2002; Greenhill *et al.* 2003a; Braatz *et al.* 2004; Henkel *et al.* 2005; Kondratko *et al.* 2006a,b; Yamauchi *et al.* 2017). The 22 GHz H_2O megamaser emission coming from AGN-illuminated innermost molecular gas has been used to probe gas dynamics in close proximity to central mass-accreting SMBHs and accurately measure the SMBH masses, based on follow-up centimeter VLBI (very long baseline interferometry) high-angular-resolution observations (e.g., Miyoshi *et al.* 1995; Greenhill *et al.* 1997, 2003b). Although this method is very powerful, it is applicable only to AGNs with extremely bright 22 GHz H_2O megamaser emission (e.g., Kuo *et al.* 2011, 2020a). SMBH mass in the ULIRG population has never been estimated in this method.

3.3. *(Sub)millimeter H_2O magamaser emission*

Imanishi *et al.* (2021) have recently detected a remarkably luminous (>$10^4L_\odot$) 183 GHz (1.6 mm) H_2O $3_{1,3}$–$2_{2,0}$ emission line in the merging ULIRG, the Superantennae (IRAS 19254−7245; $z = 0.0617$; 1″ = 1.2 kpc) (Figure 4). The detected 183 GHz H_2O emission line is unusually bright, even brighter than widely used major dense molecular gas tracers, HCN, HCO^+, and HNC J=2–1 lines (Figure 4a–b). Additionally, while emission of dense molecular gas tracers is spatially resolved with 500 pc beam-sized data (Figure 5a–b), the 183 GHz H_2O emission is not (Figure 5c), suggesting that the bright 183 GHz H_2O emission line comes from a very compact region. The most natural interpretation for the remarkably luminous, compact 183 GHz H_2O emission line is that we see 183 GHz H_2O *megamaser* emission in the AGN-illuminated innermost warm and dense molecular gas at the very center of the galaxy nucleus (Imanishi *et al.* 2021), as was detected in other very nearby (<20 Mpc) AGNs (Humphreys *et al.* 2005, 2016). No 22-GHz (1.4 cm) H_2O megamaser emission line was detected in the Superantennae (Greenhill *et al.* 2002).

Subsequent ALMA higher-spatial-resolution (∼60 pc beam) data revealed redshifted and blueshifted components at ∼100 pc scale for the 183 GHz H_2O emission line, suggesting that it is barely spatially resolved in the Superantennae (Figure 5d and 4c). Figure 6 shows a schematic diagram of the geometrical difference between the 183 GHz H_2O and dense molecular line emission in the Superantennae. Given that the 183 GHz H_2O megamaser emission selectively comes from the innermost region around a mass-accreting SMBH, this megamaser (non thermal) emission can be a more reliable tool to dynamically constrain the central SMBH mass than using spatially extended (∼kpc) thermal

https://doi.org/10.1017/S1743921323002478 Published online by Cambridge University Press

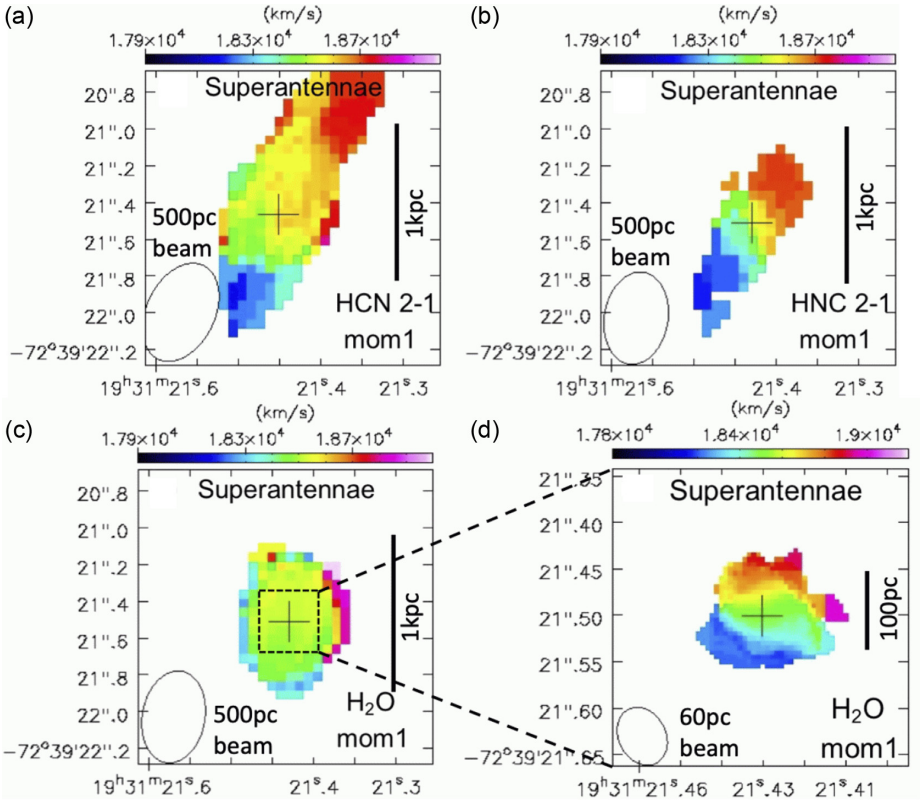

Figure 5. Intensity-weighted mean velocity (moment 1) map of *(a)* HCN J=2–1 line, *(b)* HNC J=2–1 line, *(c)* 183 GHz H_2O line of the Superantennae (Imanishi *et al.* 2021). The vertical bar in *(a)*–*(c)* corresponds to 1 kpc. Dense molecular gas tracers (HCN and HNC J=2–1 lines) display rotation pattern with north-western redshifted and south-eastern blueshifted components, because these lines are spatially resolved with ∼500 pc beam. However, no such rotation signature is seen for the 183 GHz H_2O emission line, strongly suggesting that it is spatially unresolved (<220 pc). In *(d)*, a newly taken ∼60 pc beam-sized moment 1 map of the 183 GHz H_2O line (Imanishi *et al.* 2023b in preparation) is displayed. The vertical bar in *(d)* corresponds to 100 pc. The compact 183 GHz H_2O emission is spatially resolved at ∼100 pc scale, with north redshifted and south blueshifted components discernible.

(non maser) molecular line emission. From the redshifted and blueshifted components of the 183 GHz H_2O emission line (Figure 5d), enclosed mass is roughly estimated to be $\sim 10^8 M_\odot$, by assuming a simple Keplerian rotation. This is comparable to *inferred* SMBH masses in nearby ULIRGs ($M_{SMBH} = 10^{7-8} M_\odot$) from host galaxies' stellar properties (e.g., Genzel *et al.* 2001; Dasyra *et al.* 2006), although even smaller ALMA beam size is ultimately needed to better estimate the M_{SMBH} value. The *extremely bright, compact (<<1 kpc) AGN-origin 183 GHz H_2O megamaser emission* (Figure 6) *can provide the best achievable constraints on gas dynamics in the vicinity of mass-accreting SMBHs* in gas/dust-rich merging ULIRGs, with the smallest modeling uncertainty of spatially extended, >kpc-wide stellar and gas mass distribution (Boizelle *et al.* 2019).

3.4. *Future prospect*

To fully exploit the potential power of millimeter AGN-origin H_2O megamaser emission for the purpose of estimating SMBH mass in a more reliable manner and directly

https://doi.org/10.1017/S1743921323002478 Published online by Cambridge University Press

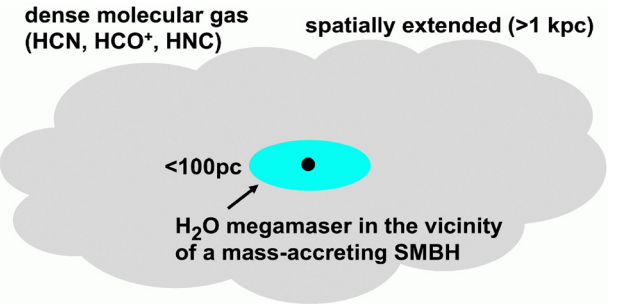

Figure 6. Schematic diagram of the H_2O megamaser emission and dense molecular gas. The AGN-origin H_2O megamaser emission comes from the very center of a galaxy nucleus (<<1 kpc), while dense molecular line emission comes from the entire nuclear region (kpc scale). Stars and low density molecular gas (probed with CO) distribute in a much wider area (>>1 kpc).

witnessing the SMBH mass growth in gas-rich galaxy mergers, we need even higher-spatial-resolution data. This is because not only the SMBH, but also gas and stars at $\lesssim$60 pc could contribute to the above estimated enclosed mass with $\sim 10^8 M_\odot$ for the Superantennae. ALMA observations of the 183 GHz H_2O megamaser emission with the longest baseline will provide a factor of $\sim$2 improvement in spatial resolution, compared to the available data for the Superantennae (Figure 5d).

In addition to the 183 GHz (1.6 mm) H_2O megamaser emission, the 321 GHz (0.9 mm) H_2O megamaser emission has been detected in nearby well-studied AGNs (e.g., Hagiwara *et al.* 2013, 2016; Pesce *et al.* 2016; Hagiwara *et al.* 2021; Kameno *et al.* 2023; Pesce *et al.* 2023). At 321 GHz (0.9 mm), even higher spatial resolution can be achieved with ALMA, because of shorter wavelength than at 183 GHz (1.6 mm). The smallest achievable angular resolution of ALMA at 321 GHz is $\lesssim 0.015''$ or as small as $\lesssim$18 pc for the Superantennae at $z \sim 0.06$. Because AGNs show bright H_2O megamaser emission at multiple lines, and not at only one line (Pesce *et al.* 2023), it is quite possible that bright AGN-origin 321 GHz H_2O megamaser emission is detected in the Superantennae. If we can detect bright, AGN-origin, compact 321 GHz H_2O megamaser emission in the Superantennae at $z \sim 0.06$, we should be able to constrain the central SMBH mass if it is $M_{SMBH} \gtrsim 5 \times 10^7 M_\odot$ (Davis 2014), given that the H_2O megamaser emitting disk in the Superantennae is highly edge-on as suggested from the spatially separated redshifted and blueshifted emission components (Figure 5d).

It is also very important to detect bright 183 GHz and/or 321 GHz H_2O megamaser emission lines in other moderately nearby ($z \lesssim 0.1$) ULIRGs as well, to verify the widely argued SMBH mass growth scenario in gas-rich galaxy mergers in more general. Previously conducted centimeter surveys of bright 22 GHz (1.4 cm) H_2O megamaser emission have shown that the megamaser detection rate can be as high as $\sim$50% if we target highly *obscured AGNs* (e.g., Panessa *et al.* 2020; Kuo *et al.* 2020a). It is quite possible that we will be able to detect bright 321 GHz (0.9 mm) and/or 183 GHz (1.6 mm) H_2O megamaser emission in multiple $z \lesssim 0.1$ ULIRGs hosting luminous obscured AGNs, if we can conduct the (sub)millimeter H_2O megamaser emission line survey. Once we can detect bright AGN-origin 321 GHz (0.9 mm) H_2O megamaser emission, then by using the highest achievable angular resolution with ALMA at 321 GHz ($\lesssim 0.015''$), we should be able to constrain SMBH mass in ULIRGs at $z \sim 0.1$, if the mass is $M_{SMBH} \gtrsim 6 \times 10^7 M_\odot$ (unless an H_2O megamaser emitting disk is highly face-on) (Davis 2014). High-spatial-resolution and high-sensitivity ALMA observations at (sub)millimeter wavelength will play a key role to most stringently test the SMBH mass growth scenario in gas-rich galaxy mergers in the universe.

https://doi.org/10.1017/S1743921323002478 Published online by Cambridge University Press

4. Summary

We demonstrated from our infrared and (sub)millimeter spectroscopic observations that luminous buried AGNs are common and so SMBH mass growth is ongoing in nearby ($z < 0.3$) gas/dust-rich merging ULIRGs. It is awaited to constrain the central SMBH masses in the nearby ULIRG population at almost-extinction-free wavelengths, by penetrating through a large column density of nuclear obscuring material, to test the widely proposed SMBH mass growth scenario in gas-rich galaxy mergers. We argued that ALMA high-spatial-resolution and high-sensitivity observations of bright AGN-origin (sub)millimeter H_2O megamaser emission lines can be the most unique tool to achieve this goal, which is vital to understand the origin of the co-evolution of SMBHs and stars in our universe.

5. Acknowledgment

The author of this manuscript (M.I.) is supported by JP21K03632.

References

Aladro, R., Martin, S., Riquelme, D., *et al.* 2015, *A&A*, 579, A101
Alonso-Herrero, A., Ward, M. J., & Kotilainen, J. K. 1997, *MNRAS*, 288, 977
Armus, L., Charmandaris, V., Bernard-Salas, J., *et al.* 2007, *ApJ*, 656, 148
Baldwin, J. A., Phillips, M. M., & Terlevich, R. 1981, *PASP*, 93, 5
Bardeen, J. M. 1970, *Nature*, 226, 64
Boizelle, B. D., Barth, A. J., Walsh, J. L., *et al.* 2019, *ApJ*, 881, 10
Braatz, J. A., Henkel, C., Greenhill, L. J., Moran, J. M., & Wilson, A. S. 2004, *ApJ*, 617, L29
Braatz, J. A., Wilson, A. S., & Henkel, C. 1997, *ApJS*, 110, 321
Burtscher, L., Orban de Xivry, G., Davies, R. I., *et al.* 2015, *A&A*, 578, 47
Butterworth, J., Holdship, J., Viti, S., & Garcia-Burillo, S. 2022, *A&A*, 667, A131
Dasyra, K. M., Tacconi, L. J., Davies, R. I., *et al.* 2006, *ApJ*, 651, 835
Davis, T. A., 2014, *MNRAS*, 443, 911
DeBuhr, J., Quataert, E., & Ma, C-P. 2011, *MNRAS*, 412, 1341
Diaz-Santos, T., Charmandaris, V., Armus, L., *et al.* 2010, *ApJ*, 723, 993
Downes, D., & Eckart, A. 2007, *A&A*, 468, L57
Ferrarese, L., & Merritt, D. 2000, *ApJ*, 539, L9
Gao, Y., & Solomon, P. M. 2004, *ApJS*, 152, 63
Genzel, R., Lutz, D., Sturm, E., *et al.* 1998, *ApJ*, 498, 579
Genzel, R., Tacconi, L. J., Rigopoulou, D., *et al.* 2001, *ApJ*, 563, 527
Gonzalez-Alfonso, E., Fischer, J., Isaak, K., *et al.* 2010, *A&A*, 518, L43
Gonzalez-Alfonso, E., Fischer, J., Sturm, E., *et al.* 2015, *ApJ*, 800, 69
Gray, M. D., Baudry, A., Richards, A. M. S., *et al.* 2016, *MNRAS*, 456, 374
Greenhill, L. J., Booth, R. S., Ellingsen, S. P., *et al.* 2003a, *ApJ*, 590, 162
Greenhill, L. J., Ellingsen, S. P., Norris, R. P., *et al.* 2002, *ApJ*, 565, 836
Greenhill, L. J., Gwinn, C. R., Antonucci, R., & Barvainis, R. 1996, *ApJ*, 472, L21
Greenhill, L. J., Kondratko, P. T., Lovell, J. E. J., *et al.* 2003b, *ApJ*, 582, L11
Greenhill, L. J., Moran, J. M., & Herrnstein, J. R. 1997, *ApJ*, 481, L23
Hagiwara, Y., Diamond, P. J., & Miyoshi, M. 2002, *A&A*, 383, 65
Hagiwara, Y., Horiuchi, S., Doi, A., Miyoshi, M., & Edwards, P. G. 2016, *ApJ*, 827, 69,
Hagiwara, Y., Horiuchi, S., Imanishi, M., & Edwards, P. G. 2021, *ApJ*, 923, 251
Hagiwara, Y., Miyoshi, M., Doi, A., & Horiuchi, S. 2013, *ApJ*, 768, L38
Harada, N., Herbst, E., & Wakelam, V. 2010, *ApJ*, 721, 1570
Henkel, C., Peck, A. B., Tarchi, A., *et al.* 2005, *A&A*, 436, 75
Hildebrand, R. H. 1983, *QJRAS*, 24, 267
Hopkins, P. F., Hernquist, L., Cox, T. J., *et al.* 2005, *ApJ*, 630, 705
Hopkins, P. F., Hernquist, L., Cox, T. J., *et al.* 2006, *ApJS*, 163, 1
Hopkins, P. F., Hernquist, L., Cox, T. J., & Keres, D. 2008, *ApJS*, 175, 356

Humphreys, E. M. L. Greenhill, L. J., Reid, M. J., *et al.* 2005, *ApJ*, 634, L133
Humphreys, E. M. L., Vlemmings, W. H. T., Impellizzeri, C. M. V., *et al.* 2016, *A&A*, 592, L13
Ichikawa, K., Ricci, C., Ueda, Y., *et al.* 2019, *ApJ*, 870, 31
Imanishi, M. 2009, *ApJ*, 694, 751
Imanishi, M., Baba, S., Nakanishi, K., & Izumi, T. 2023, *ApJ*, 950, 75
Imanishi, M., Dudley, C. C., & Maloney, P. R. 2006a, *ApJ*, 637, 114
Imanishi, M., Dudley, C. C., Maiolino, R., *et al.* 2007a, *ApJS*, 171, 72
Imanishi, M., Hagiwara, Y., Horiuchi, S., Izumi, T., & Nakanishi, K. 2021, *MNRAS*, 502, L79
Imanishi, M., Imase, K., Oi, N., & Ichikawa, K. 2011, *AJ*, 141, 156
Imanishi, M., Maiolino, R., & Nakagawa, T. 2010b, *ApJ*, 709, 801
Imanishi, M., Nakagawa, T., Ohyama, Y., *et al.* 2008, *PASJ*, 60, S489
Imanishi, M., Nakagawa, T., Shirahata, M., Ohyama, Y., & Onaka, T. 2010a, *ApJ*, 721, 1233
Imanishi, M., Nakanishi, K., & Izumi, T. 2016a, *ApJ*, 825, 44
Imanishi, M., Nakanishi, K., & Izumi, T. 2016b, *AJ*, 152, 218
Imanishi, M., Nakanishi, K., & Izumi, T. 2018, *ApJ*, 856, 143
Imanishi, M., Nakanishi, K., & Izumi, T. 2019, *ApJS*, 241, 19
Imanishi, M., Nakanishi, K., Izumi, T., & Baba, S., 2022, *ApJ*, 926, 159
Imanishi, M., Nakanishi, K., & Kohno, K. 2006b, *AJ*, 131, 2888
Imanishi, M., Nakanishi, K., Tamura, Y., Oi, N., & Kohno, K. 2007b, *AJ*, 134, 2366
Imanishi, M., Nakanishi, K., Tamura, Y., & Peng, C. -H. 2009, *AJ*, 137, 3581
Imanishi, M., Nguyen, D. D., Wada, K., *et al.* 2020, *ApJ*, 902, 99
Izumi, T., Kohno, K., Aalto, S., *et al.* 2016, *ApJ*, 818, 42
Izumi, T., Kohno, K., Martin, S., *et al.* 2013, *PASJ*, 65, 100
Kameno, S., Harikane, Y., Sawada-Satoh, S., *et al.* 2023, *PASJ*, 75, L1
Kameno, S., Sawada-Satoh, S., Impellizzeri, C. M. V., *et al.* 2020, *ApJ*, 895, 73
Kauffmann, G., Heckman, T. M., Tremonti, C., *et al.* 2003, *MNRAS*, 346, 1055
Kewley, L. J., Heisler, C. A., Dopita, M. A., & Lumsden, S. 2001, *ApJS*, 132, 37
Kohno, K. 2005, in AIP Conf. Ser. 783, The Evolution of Starbursts, ed. S. Hüttemeister, E. Manthey, D. Bomans, & K. Weis (New York: AIP), 203 (astro-ph/0508420)
Kondratko, P. T., Greenhill, L. J., & Moran, J. M. 2006a, *ApJ*, 652, 136
Kondratko, P. T., Greenhill, L. J., Moran, J. M., *et al.* 2006b, *ApJ*, 638, 100
Kormendy, J., & Ho, L. C. 2013, *ARAA*, 51, 511
Krips, M., Neri, R., Garcia-Burillo, S., *et al.* 2008, *ApJ*, 677, 262
Kuo, C. Y., Braatz, J. A., Condon, J. J., *et al.* 2011, *ApJ*, 727, 20
Kuo, C. Y., Braatz, J. A., Impellizzeri, C. M. V., et al. 2020a, *MNRAS*, 498, 1609
Kuo, C. Y., Hsiang, J. Y., Chung, H. H., *et al.* 2020b, *ApJ*, 892, 18
Leroy, A., Evans, A., Momjian, E., *et al.* 2011, *ApJ*L, 739, L25
Magorrian, J., *et al.* 1998, *ApJ*, 115, 2285
Maloney, P. R. 2002, *PASA*, 19, 401
Matsushita, S., Iono, D., Petitpas, G. R., *et al.* 2009, *ApJ*, 693, 56
McConnell, N. J. & Ma, C-P. 2013, *ApJ*, 764, 184
Meijerink, R., Spaans, M., & Israel, F. P. 2007, *A&A*, 461, 793
Miyoshi, M., Moran, J., & Herrnstein, J., *et al.* 1995, *Nature*, 373, 127
Murphy, E. J., Stierwalt, S., Armus, L., *et al.* 2013, *ApJ*, 768, 2
Nakajima, T., Takano, S., Kohno, K., Harada, N., & Herbst, E. 2018, *PASJ*, 70, 7
Nardini, E., Risaliti, G., Salvati, M., *et al.* 2008, *MNRAS*, 385, L130
Nardini, E., Risaliti, G., Salvati, M., *et al.* 2009, *MNRAS*, 399, 1373
Nardini, E., Risaliti, G., Watabe, Y., Salvati, M., & Sani, E. 2010, *MNRAS*, 405, 2505
Neufeld, D. A., & Melnick, G. J. 1991, *ApJ*, 368, 215
Oda, S., Tanimoto, A., Ueda, Y., *et al.* 2017, *ApJ*, 835, 179
Panessa, F., Castangia, P., Malizia, A., *et al.* 2020, *A&A*, 641, A162
Pereira-Santaella, M., Colina, L., Garcia-Burillo, S., *et al.* 2021, *A&A*, 651, A42
Pesce, D. W., Braatz, J. A., & Impellizzeri, C. M. V., 2016, *ApJ*, 827, 68

Pesce, D. W., Braatz, J. A., Henkel, C., *et al.* 2023, *ApJ*, submitted (arXiv:2302.02572)
Predehl, P., & Schmitt, J. H. M. M. 1995, *A&A*, 293, 889
Privon, G. C., Herrero-Illana, R., Evans, A. S., *et al.* 2015, *ApJ*, 814, 39
Ranalli, P., Comastri, A., & Setti, G. 2003, *A&A*, 399, 39
Ricci, C., Bauer, F. E., Treister, E., *et al.* 2016, *ApJ*, 819, 4
Ricci, C., Bauer, F. E., Treister, E., *et al.* 2017, *MNRAS*, 468, 1273
Ryter, C. E. 1996, *Ap&SS*, 236, 285
Saito, T., Iono, D., Ueda, J., *et al.* 2018, *MNRAS*, 475, L52
Sakamoto, K., Gonzalez-Alfonso, E., Martin, S., *et al.* 2021, *ApJ*, 923, 206
Sakamoto, K., Wang, J., Wiedner, M. C., *et al.* 2008, *ApJ*, 684, 957
Sanders, D. B., & Mirabel, I. F. 1996, *ARAA*, 34, 749
Scoville, N., Murchikova, L., Walter, F., *et al.* 2017, *ApJ*, 836, 66
Shang, Z., Brotherton, M. S., Wills, B. J., *et al.* 2011, *ApJ*, 196, 2
Soifer, B. T., Neugebauer, G., Matthews, K., *et al.* 2000, *AJ*, 119, 509
Takano, S., Nakajima, T., & Kohno, K. 2019, *PASJ*, 71, S20
Teng, S. H., Rigby, J. R., Stern, D., *et al.* 2015, *ApJ*, 814, 56
Thompson, T. A., Quataert, E., & Murray, N. 2005, *ApJ*, 630, 167
Thorne, K. S. 1974, *ApJ*, 191, 507
Veilleux, S., & Osterbrock, D. E. 1987, *ApJS*, 63, 295
Veilleux, S., Rupke, D. S. N., Kim, D.-C., *et al.* 2009, *ApJS*, 182, 628
Yamada, S., Ueda, Y., Tanimoto, A., *et al.* 2021, *ApJS*, 257, 61
Yamauchi, A., Miyamoto, Y., Nakai, N., *et al.* 2017, *PASJ*, 69, L6
Yates, J. A., Field, D., & Gray, M. D. 1997, *MNRAS*, 285, 303
White, S. D. M., & Rees, M. J. 1978, *MNRAS*, 183, 341
Wilms, J., Allen, A., & McCray, R. 2000, *ApJ*, 542, 914

https://doi.org/10.1017/S1743921323002478 Published online by Cambridge University Press